J Polym Res (2017) 24: 60
DOI 10.1007/s10965-017-1224-5

ORIGINAL PAPER

Preparation of carboxymethyl chitosan nanofibers through electrospinning the ball-milled nanopowders with poly (lactic acid) and the blood compatibility of the electrospun NCMC/PLA mats

Ju Lv[1] · Xueqiong Yin[1,2] · Qinhuan Zeng[1] · Wenyuan Dong[1] · Haifang Liu[3] · Li Zhu[1]

Received: 6 September 2016 / Accepted: 19 March 2017 / Published online: 23 March 2017

Abstract Carboxymethyl chitosan was pulverized to nanopowder (NCMC) with a diameter of 483 nm through ball-milling. 400 mg NCMC was successfully electrospun to nanofibers with the assistant of 4 g poly (lactic acid) (PLA) to prepare NCMC/PLA nanofibrous composite mats. Scanning electron microscope images revealed that there were no NCMC particles in the NCMC/PLA mats, indicating NCMC had been stretched to nanofibers. NCMC/PLA mats with different morphology could be prepared through adjusting the electrospinning voltage at 12–30 kV and the distance at 10–22 cm. The presence of NCMC increased the spinnability of PLA according to the electrospinning parameters. X-ray photoelectron spectroscopy and Fourier transform infrared spectroscopy verified the existence of NCMC in the mats. Crosslinking with glutaraldehyde increased the stability of NCMC/PLA in water. Crosslinked NCMC/PLA mats expressed good blood compatibility according to the results of blood clotting time and platelet adhesion experiment. The methodology of preparation nanofibers from polymer nanopowders through electrospinning could be used to prepare more composite nanofibers while adopting different raw materials.

✉ Xueqiong Yin
yxq88@hotmail.com

[1] Hainan Provincial Fine Chemical Engineering Research Center, Hainan University, Haikou, Hainan 570228, People's Republic of China

[2] School of Materials and Chemical Engineering, Hainan University, 58th Renmin Road, Haikou, Hainan 570228, People's Republic of China

[3] Affiliated Haikou Hospital, Xiangya School of Medicine Central South University, Haikou Municipal People's Hospital, Haikou, Hainan 570208, People's Republic of China

Keywords Carboxymethyl chitosan nanopowder · Electrospin · Nanofiber · Poly (lactic acid) · Blood compatibility

Introduction

Biomaterial is a substance used to fulfill medical purposes, therapeutically or diagnostically. Up to now, many kinds of biomaterials, such as metallic components, polymers, ceramics, and composite materials have been applied in clinic [1]. A successful biomaterial should be biocompatible, not eliciting local or systemic responses from a living system or tissue [2]. For many biomaterials, blood is the first body fluid they contact in human body. When a foreign material gets contact with blood, plasma proteins (mainly serum albumin, globulin, fibrinogen, prothrombin) are rapidly absorbed onto the material surface. Those adsorbed proteins will bind to platelets and induce platelet adhesion and aggregation, which leads to blood clotting [3, 4]. To achieve good blood compatibility, the characteristics of material surface(such as chemical components, morphology, surface charge, surface wettability, etc.)are usually designed to modulate the process of protein adsorption and platelet activation.

Chitosan (poly-β-1,4-D-glucosamine) is the N-deacetylated derivative of chitin. Chitosan is the only natural basic polysaccharide, which has good biocompatibility, biodegradability, antibacterial and antifungal activities, and many biological properties [5]. Moreover, the structural similarity with glycosaminoglycans, one of the natural extracellular matrixes (ECM), enables chitosan potential to be used as biomaterials. However, up to now, the blood compatibility of chitosan is still controversial. On one hand, positively charged chitosan is easy to adsorb negative proteins which cause platelets activation and thrombus formation. Moreover, chitosan could activate the complement

system and the intrinsic pathway of coagulation [6]. On the other hand, chitosan prefers binding human serum albumin, which reduces platelet attachment and activation [7]. To increase the blood compatibility of chitosan, chitosan derivatives, composites, and chitosan with different visual structure have been prepared [6–8]. It is revealed that chitosan derivatives with negative $–SO_3^-$ or $–COO^-$ group have good blood compatibility due to their negative charges decrease the adsorption of negative plasma proteins [7, 9, 10]. Carboxymethyl chitosan (CMC) is the most popular derivative of chitosan, which has been widely researched in biomaterials. It has been reported that CMC had no significant effects on the blood system of rats and can be used safely [11]. CMC has been used to modify other polymers to improve the blood compatibility [12]. However, more details on the blood compatibility of CMC with different structure and morphology have not been reported. It is necessary to investigated it to develop the application of CMC in blood-contacting materials.

Electrospinning is an effective methodology for preparing materials with designed chemical structure and morphology [13, 14]. Electrospun mats have been widely researched in the field of blood-contacting biomaterials, such as would healing materials, drug delivery, medical textiles, tissue engineering scaffolds, etc. [15]. During the process of electrospinning, a high voltage is first applied to the solution droplet at the nozzle. The droplet is charged and undergoes an electrostatic repulsion force. At a critical point which is called Taylor cone, the electrostatic repulsion force overcomes the surface tension of the solution, and then the solution is ejected out the nozzle. The solution flies to and finally deposits onto the grounded collector. Very fine fibers (in the scale of micrometers or nanometers) are obtained on the collector after the solvent evaporating during solution flying [16]. Electrospun mats with designed surface structure could be prepared while adjusting the polymer properties (components, molecular weight, viscosity, solution concentration, etc.), electrospinning parameters (voltage, flow rate, distance, collector type, etc.), and electrospinning mode (single spinning fluid or multiple spinning fluids, coaxial electrospinning, etc.) [17, 18]. Electrospinning of chitosan and carboxymethyl chitosan has been investigated in recent years. Owing to the strong molecular interactions between the highly charged density and high viscosity of chitosan and CMC solutions, it is very difficult to electrospin chitosan or CMC solely [19]. Other polymers which have flexible polymer chains and could be electrospun easily, such as poly (lactic acid), poly (vinyl alcohol), polyethylene oxide, etc., have been used to facilitate the electrospinning of chitosan and chitosan derivatives to prepare nanofibers [20–23]. Usually, chitosan or its derivatives should be dissolved in specific solvent and blended with the polymer solution before electrospinning. The process is still affected by polymer dissolution and the solution properties. And the use of additional solvent increases the risk of environment pollution. New electrospinning technology for chitosan and its derivatives are still in demand.

Poly (lactic acid) (PLA, $-[CH(CH_3)COO]_n-$) is a linear biodegradable aliphatic polyester, which could be prepared from renewable bioresources through fermentation and polymerization. PLA has been approved by FDA to be applied in biomaterials, such as sutures, bone plates, abdominal mesh, and drug delivery [24, 25]. However, the blood compatibility of PLA is not good enough to meet the requirements of many blood-contacting materials [26]. Many methodologies have been tried to increase its blood compatibility, such as surface modification, endothelial cell seeding, surface morphology fabrication, etc. [27–29]. Electrospinning with other chemicals (such as chitosan derivatives) is one of the methodologies to fabricate blood compatible PLA material with specific chemical components and morphology [30, 31].

Ball-milling is one kind of ultrafine milling, which is widely used to grind materials, such as coal, pigments, ores, food fibers, etc., down to very small sizes (1 μm–100 μm, sometimes even in nanoscales). Chitosan has been successfully micronized by ball-milling to prepare nanopowders [32], while CMC has not been reported to be ball-milled. Nanopowders, mostly inorganic nanopowders have been applied in electrospinning to prepare composites, in which the nanopowders still keep the shape of powders [33]. Up to now, there has no report on electrospinning of polymer nanopowders. Direct electrospinning of CMC powders has not been reported, either. CMC is a highly negtively charged polymer. It is possible to stretch CMC nanopowder (NCMC) to threads or even nanofibers through electrospinning in a high voltage electrostatic field. Therefore, in this paper, CMC was first ball-milled to prepare NCMC. Then NCMC was electrospun together with PLA solution to prepare CMC/PLA nanofibrous mats (NCMC/PLA). The mats were characterized with X-ray photoelectron spectroscopy (XPS), Scanning electron microscopy (SEM), Fourier transform infrared spectroscopy (FTIR), and water contact angles. The blood compatibility of NCMC/PLA mats was measured through clotting times and platelet adhesion experiment. The APTT of PLA was prolonged by NCMC. The new methodology supplied here could be used to prepare polymer composites with designed structure and morphology through electrospinning.

Experimental

Materials

CMC was purchased from Bomeibo Co., Ltd. (Mw 3.4×10^5 g/mol, DD > 90%,particle size 2.3 μm). Poly (lactic acid) (PLA4032D, Mw 1.67×10^5 g/mol) was purchased from Nature Works LLC. NaH_2PO_4, $NaH(PO_4)_2$, and 50%

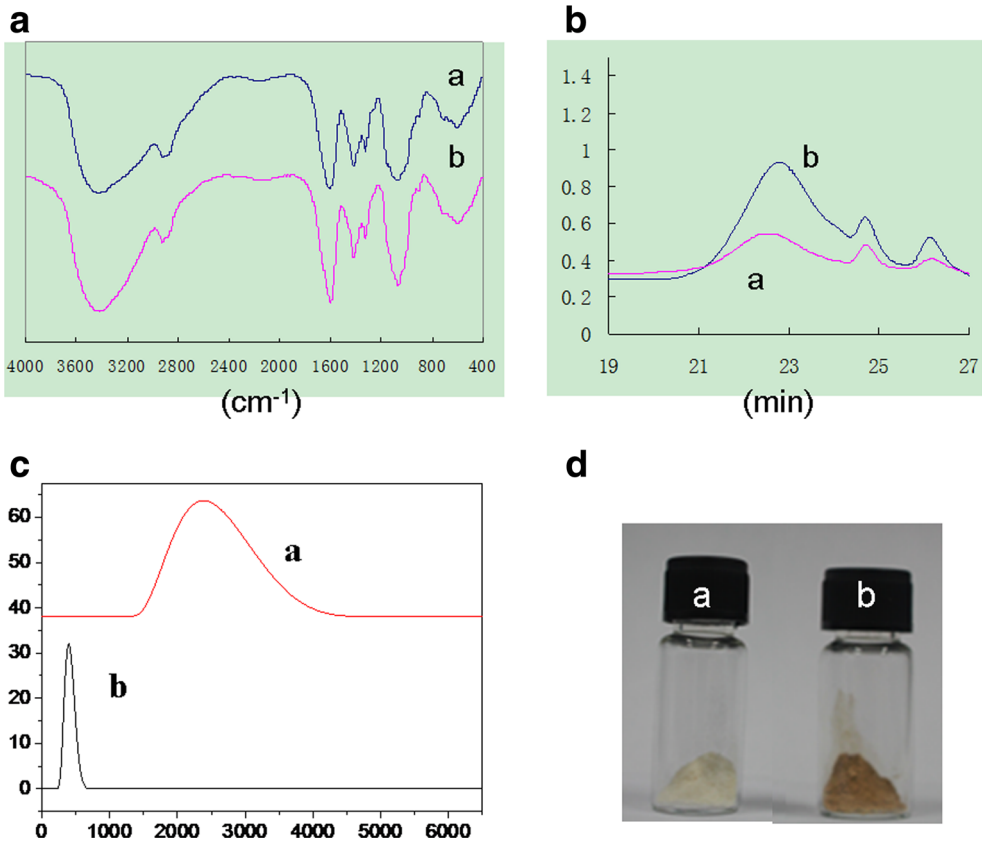

Fig. 1 Structure characterization of the original CMC (*a*) and NCMC (*b*) (FTIR spectra **a**; GPC curves **b**; particle size distribution **c**; visual images **d**)

glutaraldehyde solution were purchased from Sinopharm Group Co., Ltd. (China). All the reagents were used as received.

Preparation of NCMC

After vacuum dried at 90 °C overnight, 400 mg CMC was put into a MM400 ball mill (Retsch GmbH, Germany). CMC was micronized by 2 steel balls with a diameter of 10 mm for 4 h at 20 Hz to get NCMC. NCMC was taken out and characterized. The nanopowder were measured with FTIR on a TENSOR 27 spectrometer in the range of 500 ~ 4000 cm^{-1}. Particle size distribution of NCMC was determined using the laser scattering method on a Zetasizer Nano S90 laser diffractometer (Malvern Instrument Co., Southborough, UK) equipped with a He-Ne laser (wavelength 633 nm). Before the measurement, the NCMC sample was ultrasonically dispersed in ethanol.

Preparation and crosslinking of the electrospun NCMC/PLA mats

4 g PLA was put into 50 mL mixture of N,N-dimethylformamide and dichloromethane (7: 3 (v: v)). 8 wt% PLA was obtained after stirring for 2 h. 400 mg of NCMC was put into 50 mL 8 wt% PLA with magnetic stirring to prepare the solution for further electrospinning. The electrospinning experiment was carried out on an electrostatic spinning instrument (DT-200, Dalian Dingtong Technology Development Co., Ltd.). In a typical procedure, the electrospinning solution was put into a 25 mL syringe and then delivered to the tip of the syringe needle by the syringe pump at a constant feed rate. A positive voltage was applied to the polymer solution via a stainless steel syringe needle. The distance between the injector and the collector was maintained at 10–22 cm. The electrospun polymer fibers were collected on a collector covered with aluminum foil.

The NCMC/PLA mats were crosslinked in 50% glutaraldehyde aqueous solution at 80 °C for 12 h. After crosslinking, the mats were treated with a 0.1 mol/L glycine aqueous solution to block unreacted aldehyde groups. And then the mats were put in an oven at 60 °C for 2 days. The dried mats were put into distilled water in a 50 mL beaker. Put the beaker in a water bath at 37 °C for 30 min. The mats were taken out and dried in a vacuum oven at 60 °C for 2 days.

Characterization of NCMC/PLA mats

The surface morphology of the NCMC/PLA mats was observed with a S-3000 N scanning electron microscope (Hitachi, Japan) after gold coating at the voltage of 10 kV. The water contact angle of the mats was measured on a SL200K contact angle measurement instrument at 20 °C. A drop of deionized water was dropped onto the sample surface. The contact angles were calculated using the image processing

Table 1 Electrospinning parameters and the morphology of NCMC/PLA mats

Samples	CMC (mg)	PLA (g)	Voltage (kV)	Distance (cm)	Morphology
PLA	0	4	30	22	Fibers 200 nm - 1 μm, in three dimensions
CP1	400	4	12	10	Fibers 200 nm - 2 μm, in three dimensions
CP2	400	4	12	16	Fibers 200–800 nm, in three dimensions
CP 3	400	4	18	10	Fibers 200–700 nm, some fibers in curve
CP 4	400	4	18	16	Fibers 200–500 nm, some fibers in curve
CP 5	400	4	18	22	Fibers 200–400 nm, some fibers in curve
CP 6	400	4	30	16	Violently distributed fibers

software CAST™2.0. The measurement was reproduced 10 times and the average value was adopted. The original PLA and NCMC/PLA mats were analyzed using a X-ray photoelectron spectroscope (Thermo Scientific Escalab 250Xi, England) equipped with a Al K Alpha X-ray source (powered at 10 mA and 15 kV). The spot size was 400 μm. The pass energy was set at 50 eV for the survey spectrum and the energy step size was 0.100 eV. The pressure in the analysis chamber was around 10^{-7} Pa. The elemental compositions were determined on the basis of peak areas and sensitivity factor from the C1s, N1 s, and O1s peaks by the software CasaXPS (Casa Software, Teignmouth, UK). The FTIR spectra were obtained on a TENSOR 27 spectrometer in the range of 500 ~ 4000 cm^{-1} through KBr pellet technology.

Blood compatibility measurement

Fresh human blood mixed with sodium citrate was centrifuged at 3000 r/min for 10 min to obtain platelet-poor plasma (PPP) and platelet-rich plasma (PRP). The specimens (1 cm × 1 cm) were incubated in 800 μL PPP at 37 °C for 20 min. Then, 200 μL PPP was taken to measure the in vitro coagulation times, including activated partial thrombin time (APTT) and thrombin time (TT). The measurement was carried out on a CA-50 blood coagulation analyzer (Sysmex, Japan). To investigate the platelet adhesion of NCMC/PLA mats, 250 uL PRP was poured onto the NCMC/PLA mats (0.5 cm × 0.5 cm) and allowed to maintain at 37 °C for 2 h. Then the samples were carefully washed with saline to remove the nonadhered blood cells. The adhered blood cells were fixed by immersing the mats into 20 mL 2.5 wt% solution of glutaraldehyde for 1 h at room temperature to fix the platelets. The mats were washed with PBS and then subsequently dehydrated by immersing into a series of ethanol–water solutions (50, 60, 70, 80, 90, 95, and 100% (*v*/v)) for 30 min each and allowed to evaporate at room temperature. The samples were dried for further operation. The surface of the mats was observed with a JSM-7100F field emission scanning electron microscope (JOEL, Japan) after gold coating.

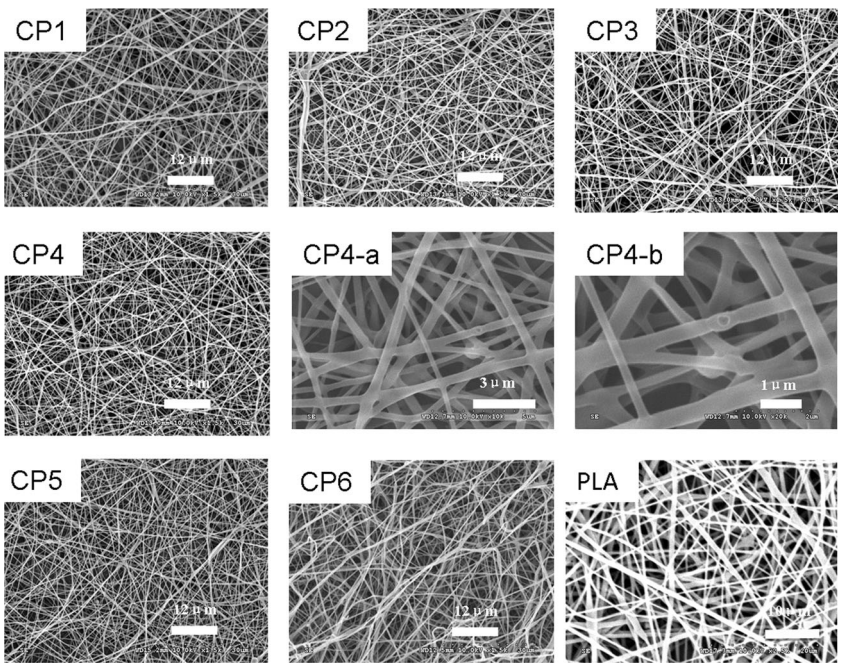

Fig. 2 SEM images of NCMC/PLA prepared at differnt conditions and SEM images of CP4 at different mangnification (CP4, 1500; CP4-a, ×10,000; CP4-b × 20,000)

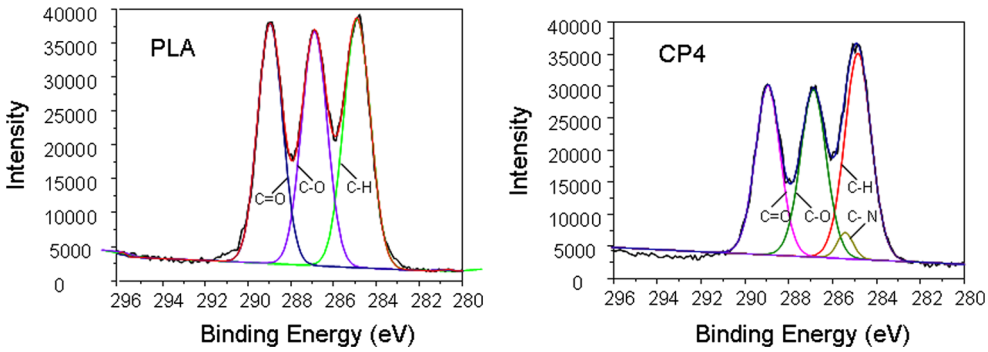

Fig. 3 XPS spectra of PLA and CP4

Results and discussion

Preparation and characterization of NCMC

CMC was ball-milled at 20 Hz in a MM400 ball mill (Retsch GmbH) for 4 h to prepare NCMC. The structure characterization results of the original CMC (a) and NCMC (b) (FTIR spectra (A), GPC curves (B), particle size distribution (C), visual images (D)) were shown in Fig. 1. As shown in Fig. 1a, the FTIR spectra had no change after ball milling, which indicated that there was no obvious structure change during ball-milling. Ball-milling caused depolymerization of CMC. After ball-milling, the molecular weight of CMC decreased from 1.4×10^5 to 0.5×10^5 according to the GPC results (Fig. 1b), and the particle size of chitosan decreased from 2.3 μm to 483 nm (Fig. 1c). Compared with the original CMC powder before ball-milling (Fig. 1d), NCMC became lightly brown. During the ball-milling process, Maillard reaction might happen between the amino groups of chitosan and the carbonyl groups of the reducing ends, which resulted in the browning of NCMC [34].

Electrospinning conditions and the morphology of the NCMC/PLA mats

400 mg NCMC obtained after ball-milled for 4 h were added into 50 mL 8 wt% PLA solution for further electrospinning. The electrospinning parameters (electrospinning voltage and the distance from the injector to the collector) and the morphology of NCMC/PLA mats were shown in Table 1.

As shown in Table 1 and Fig. 2, NCMC/PLA with only fibers could be obtained at different voltages and distances. The morphology of NCMC/PLA varied in some degree with the electrospinning parameters. In the process of electrospinning, the polymer solution at the nozzle of the spinneret becomes highly electrified and gets an electrostatic force when a high voltage is applied to the system [35]. Once the electrostatic force overcomes the surface tension of the polymer solution, the liquid is ejected as a jet from the nozzle. When the jet comes out from the nozzle, it is firstly accelerated and stretched smoothly by electrostatic forces. Then, a "bending instability" occurs, and the jet follows a bending, spiraling, and looping path in three dimensions with large, irregular loops before it reaches the collector [35, 36]. The fibers with diameters from micrometers to nanometers are obtained on the collector. The electrospinning voltage and distance affect the process of stretching and bending [37]. Usually, higher voltage supplies higher electrostatic force and more stretching power, causing smaller fibers. And longer distance enables enough time for the solution to stretch and the solvent to evaporate, leading to smaller fibers. Therefore, keeping the voltage at a constant level, increasing the distance from 10 cm to 16 cm leads to fibers with smaller and evener distribution (CP1 vs. CP2 at 12 kV, CP3 vs. CP4 and CP5 at 18 kV). Keeping the injector at the same distance to the collector, while increasing the voltage from 12 kV to 18 kV, the diameters of fibers decreased and some fibers were curved (CP1 vs. CP3 at 10 cm, CP2 vs. CP4 at 16 cm). However, when the voltage is too high, there are too many charges on the surface of Taylor cone, which leads to uncertain injecting, high bending instability of the jet, and disorderly distributed fibers. Therefore, while further increasing the voltage (CP6) to 30 kV at 16 cm, the distribution of the fibers became violent, not in typical three dimensions.

Pure PLA could be electrospun to mats with only fibers at 30 kV and 22 cm. The voltage and the distance of PLA were larger than those of NCMC/PLA, indicating NCMC increased the spinnability of PLA due to negatively charged NCMC

Table 2 The attribution of the XPS peaks of PLA and CP4

Sample	PLA				CP4			
	C-H	C-N	C-O	C = O	C-H	C-N	C-O	C = O
Area (%)	35.54	0	31.30	33.16	38.27	2.45	30.07	29.21
Binding energy (eV)	284.89	0	286.89	288.96	284.84	285.42	286.87	288.95

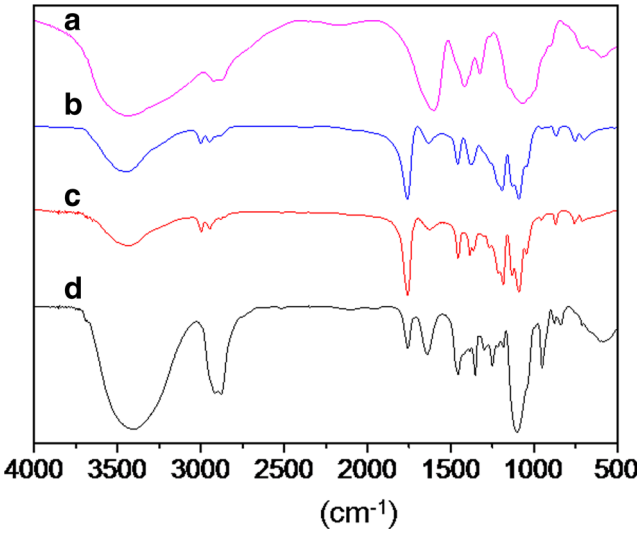

Fig. 4 FTIR spectra of NCMC **a**, PLA **b**, NCMC/PLA **c**, and glutaradehyde crosslinked NCMC/PLA **d**

increased the electric conductivity and the electrostatic force of the solution. The electrospinning parameters were similar with the solution electrospinning of CMC together with other polymers (including PVA, PEO, PAA, etc.) [21]. As shown in Fig. 2 (CP4, CP4-a, and CP4-b), no NCMC particles were observed in the SEM images at different magnification (×1500, 10,000, and 20,000). CMC is a highly negatively charged polymer. It could be stretched in high electric field. The results indicated that CMC particles with a size of 483 nm were stretched to nanofibers during electrospinning. Comparing the electrospinning technologies with dissolved CMC in literatures [19, 21], the present methodology simplifies the electrospinning process of CMC.

Structure characterization of NCMC/PLA mats

CP4 and the pure PLA mat were measured by XPS. The XPS spectra were shown in Fig. 3. In the spectrum of PLA, the C_{1s} peak showed only three components: (1) carbon bound to carbon and hydrogen [C–(C, H)] at 284.89 eV; (2) carbon making a single bond with oxygen C–O near 286.89 eV; (3) carbon of the carbonyl group [C = O] near 288.96 eV [38]. There was no N_{1s} contribution in the spectrum of PLA. Besides those peaks of C-O, C = O, C-H, there was a new peak near 285.42 eV which was attributed to C-N in the spectrum of CP4 [39]. The peak of C-N indicated that NCMC had been successfully blended with PLA in the NCMC/PLA mat. The percentages of individual peaks were determined using the peak areas of individual peaks, which were shown in Table 2. As shown in Table 2, the contents of C-O and C = O decreased and the content of C-H increased, which further proved the existence of NCMC in the electrospun NCMC/PLA mat.

Figure 4 expressed the FTIR spectra of NCMC (a), PLA(b), NCMC/PLA(c), and glutaradehyde crosslinked NCMC/PLA (d). In the spectrum of NCMC, the peak at 3410 cm^{-1} was due to the unbounded and hydrogen bonded O-H stretching vibration and amine N-H symmetrical vibration. The peaks at 2890 cm^{-1} and 2865 cm^{-1} were assigned to the C–H stretching bands. The peaks at 1590 cm^{-1} and 1410 cm^{-1} were from the asymmetric stretching of –C = O (−COONa) and the symmetry stretch vibration of COO^{-}, respectively [40]. The peaks at 1320 cm^{-1}, 1137 cm^{-1} and 1050 cm^{-1} were from C-H bending vibration, glycosidic bond C-O-C and C-O stretching vibration of NCMC, respectively [41] . In the spectrum of PLA, besides the absorption of O-H, C-O, C-H appeared at the similar places of NCMC, the C = O of the ester group appeared at 1755 cm^{-1}.

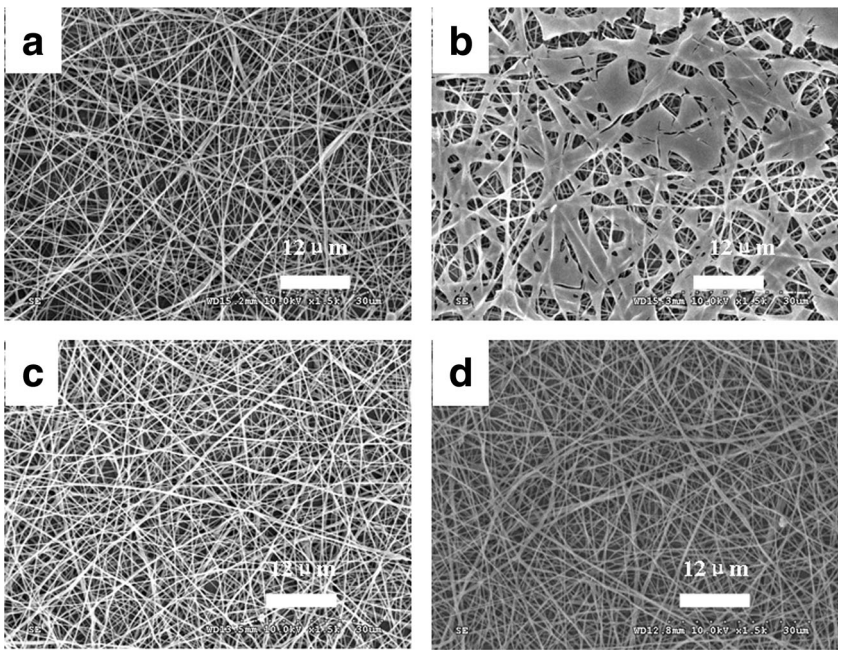

Fig. 5 SEM images of CP5 and crosslinked CP5 before and after water processing (**a** CP5 before water processing; **b** CP5 after water processing; **c** crosslinked CP5 before water processing; **d** crosslinked CP5 after water processing)

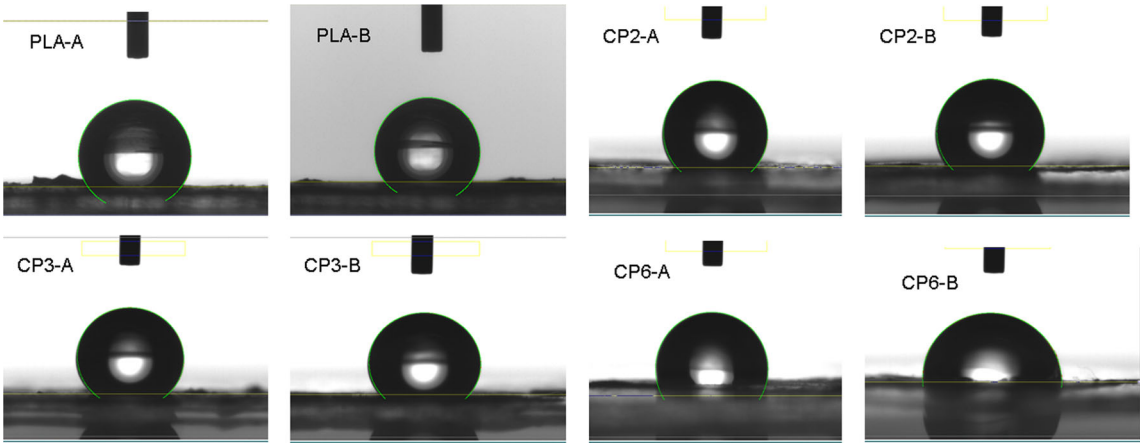

Fig. 6 Water contact angle of PLA and NCMC/PLA mats before and after crosslinking

The methyl asymmetric deformation and C-H bending vibration appeared at 1454 cm^{-1} and 1363 cm^{-1}, and the symmetric C–O–C stretching vibration of the ester group appeared at1220 cm^{-1} and 1186 cm^{-1}. The methyl rocking and C–CH_3 stretching vibration were at 1129 cm^{-1} and 1086 cm^{-1} were attributed to [42]. NCMC/PLA had the characteristic peaks of both NCMC and PLA, while the spectrum of NCMC/PLA looked more similar with that of PLA owing to much higher content of PLA in the membrane. The differences in the range of 1000–1400 cm^{-1} were owing to the overlap of peaks of NCMC and PLA. The doublets at 1383 and 1358 cm^{-1} were due to the C-H bending vibrations from PLA and NCMC. The intensity of C-O-C and C-O absorptions increased owing to the overlap of the same peaks from NCMC and PLA. The FTIR spectra of NCMC, PLA, and NCMC/PLA verified the blending of NCMC and PLA. As shown in Fig. 4b, compared with the spectrum of NCMC/PLA, the intensity of C–H stretching bands at 2890 cm^{-1} and 2865 cm^{-1} increased obviously after crosslinking, which was caused by the -$CH_2CH_2CH_2$ from glutaradehyde. The intensity of the peak at 1634 cm^{-1} also increased owing to C = N formed by Schiff reaction between carbonyl group of glutaradehyde and –NH_2 of NCMC. These changes verified the crosslinking of NCMC/PLA with glutaradehyde [43].

Table 3 Water contact angle and blood clotting times of NCMC/PLA mats

Samples	WCA −1 (°)[a]	WCA-2 (°)[b]	APTT(s)	TT(s)
control			31 ± 0.5	20.1 ± 0.3
PLA	126.4 ± 0.7	128.3 ± 1.8	28.6 ± 0.5	19.5 ± 0.2
CP2	132.6 ± 0.5	130.6 ± 0.6	31 ± 0.3	19.3 ± 0.3
CP3	137.4 ± 0.5	129.5 ± 0.6	33.3 ± 0.4	20.3 ± 0.4
CP4	132.4 ± 0.4	132.5 ± 0.5	31.2 ± 0.6	19.4 ± 0.4
CP6	118.4 ± 0.0	91.2 ± 1.8	32 ± 0.5	19.6 ± 0.4
Reference*			25--35	14--21

[a] water contact angle of NCMC/PLA before crosslinking

[b] water contact angle of NCMC/PLA after crosslinking

*the coagulation times of normal healthy people

Hydrophilicity of NCMC/PLA mats

CMC is water soluble. To make sure whether NCMC/PLA mats are suitable to be used as blood-contacting material, the images of CP5 and glutaraldehyde crosslinked CP5 after immersing in water at 37 °C for 30 min were observed with SEM. The SEM images were shown in Fig. 5, where a was CP5 before water processing; b was CP5 after water processing; c was crosslinked CP5 before water processing; d was crosslinked CP5 after water processing). As shown in Fig. 5a and b, the fibers dissolved after processing with water before crosslinking owing to the good solubility of NCMC in CP5. The image of crosslinked CP5 (c) had no obvious difference from the CP5 (a). And the morphology of crosslinked CP5 had no change after processing with water. The results indicated crosslinking with glutaraldehyde decreased the solubility of NCMC. NCMC/PLA mats kept the morphology after crosslinking with glutaraldehyde when contacting with water. The crosslinked NCMC/PLA is potential to be used in biosystem.

The water contact angles of CP2, CP3, CP4, and CP6 before and after crosslinking with glutaraldehyde were measured and shown in Fig. 6 and Table 3. The water contact angle of PLA was 126.4° due to its hydrophobic chemical structure. After crosslinking, the water contact angle of PLA increased to 128.3° owing to the existence of aliphatic chains, −C = C- groups from glutaraldehyde [44]. The water contact angles of NCMC/PLA were 118.4–137.4 ° before crosslinking, which indicated that the mats were hydrophobic [45]. After crosslinking, the water contact angles of NCMC/PLA all decreased. The wettability of membrane is affected by both the surface chemical components and the roughness of the surface. CP1-CP6 contained same amount of NCMC and PLA, while

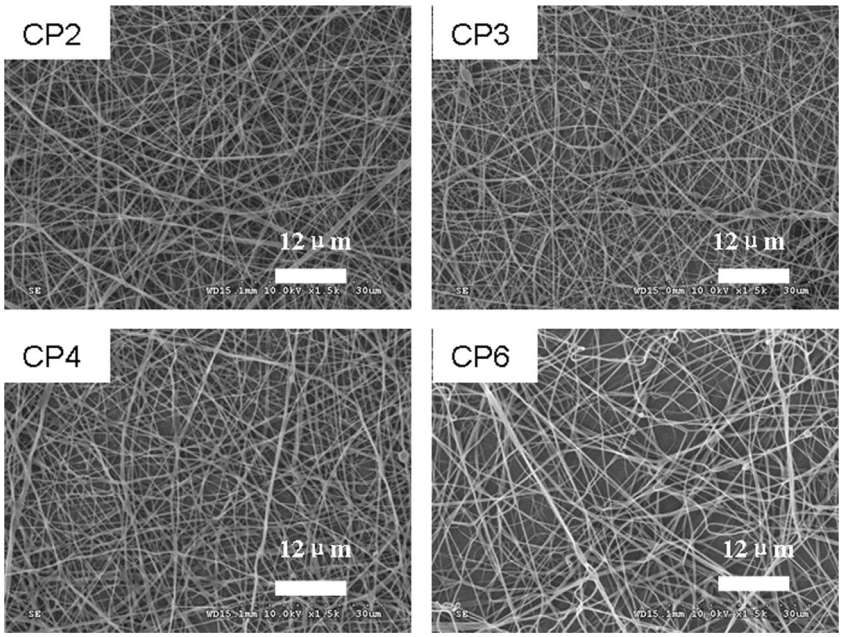

Fig. 7 SEM images of crosslinked NCMC/PLA mats

the contents of specific groups (hydrophilic –OH, −COOH, −C = O, $-NH_2$ and hydrophobic –CH, $-CH_2$) on the surface might vary owing to the difference of the electrospinning parameters. And different morphology of NCMC/PLA (shown in Fig. 2) resulted in different roughness and uneven surface of the mats. Therefore, CP1-CP6 had different water contact angles. After crosslinking, the water contact angles were supposed to increase due to more hydrophobic groups (aliphatic chains, −C = C- groups) from glutaraldehyde were introduced [44]. However, the water contact angles of CP1-CP6 decreased. The phenomena might be caused by the change of morphology after crosslinking. According to the images in Figs. 7 and 2, the morphology of NCMC/PLA mats had changed after crosslinking. The gaps among the fibers increased after crosslinking, which was most obvious for CP6. During crosslinking, the amino group of NCMC took Schiff reaction with one aldehyde group of glutaraldehyde. The hydrophobic interaction among the remained aliphatic chains of glutaraldehyde pushed the fibers away, which resulted in larger gaps among the fibers. On a micro/nano-structured surface, water droplet has three different wetting states when contacting with the surface: Wenzel state (liquid completely penetrating the

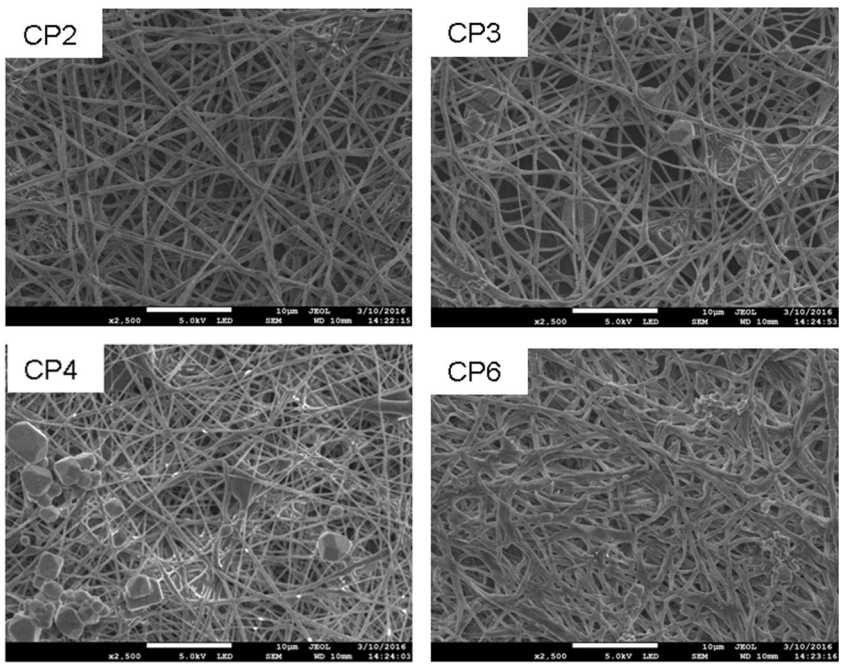

Fig. 8 SEM images of NCMC/PLA after processing with the PRP

valleys among the peaks), Cassie-Baxter state (only air existing in the valleys of the rough surfaces), and mixed Cassie-Wenzel state (partly penetrated by the liquid). The wetting state of liquid with the surface varied with the surface morphologies. For NCMC/PLA mats, the increasing of gaps among the fibers resulted in the increasing of solid-liquid contact area, and then more liquid filled the gaps between the fibers and therefore contact angles decreased [46].

Blood compatibility of NCMC/PLA mats

The blood clotting times, including APTT and TT, are widely used to evaluate the in vitro antithrombogenicity of biomaterials. APTT indicates the inhibited efficacy of both the intrinsic and the common plasma coagulation pathways. TT reflects the time of fibrinogen converting into fibrin in the PPP [47]. The in vitro clotting times APTT and TT of the samples were measured to evaluate the antithrombogenicity of NCMC/PLA mats, which were shown in Table 3. The clotting times of NCMC/PLA mats were essentially same with those of human plasma (the negative control), indicating good blood compatibility of NCMC/PLA mats [48]. The APTT of PLA (28.6 s) was shorter than that of the control (31 s), while the APTT of NCMC/PLA mats varied within 31–33.3 s. The results indicated the addition of NCMC increased the blood compatibility of PLA. This might be owing to the negative structure of NCMC decreased the adsorption of negative protein. The difference among the NCMC/PLA mats might be caused by the morphology and wettability of the mats [49].

Platelet aggregation and activation are the key factors that facilitate thrombosis and coagulation. The amount and the morphologies of the adhering platelets on material surface indicate the blood compatibility of the material [50]. Therefore, platelet adhesion experiment was carried out to measure the blood compatibility of crosslinked NCMC/PLA mats. The SEM images of NCMC/PLA mats after contacting with PRP for 2 h were shown in Fig. 8. As shown in Fig. 8, there were very few platelets absorbed on NCMC/PLA mats expect CP4 and the platelets expressed a rounded morphology with nearly no pseudopodium and deformation. There were several platelets dispersed and aggregated on the surface of CP4, while the platelets had no deformation. Many characteristics of material surface affect the interactions between the platelets and the material, such as the chemical components, morphology, hydrophilicity, etc. Platelets are regarded to have negative charges on their surfaces due to the presence of negatively charged sugar sialic acid [51]. The negatively charged NCMC in NCMC/PLA mats had electrostatic repulsion with platelets, which resulted in less absorption of platelets. CP4 had higher water contact angles and higher hydrophobicity. The hydrophobic interaction between the material surface and proteins leads to more non-specific adsorption of proteins and more platelets absorption [52]. And according to the clotting time in Table 3, CP4 is blood compatible. Therefore, though CP4 absorbed more platelets on its surface, the platelets had no activation and deformation. The platelets adhesion experiments results further verified good blood compatibility of NCMC/PLA mats.

Conclusion

A novel electrospinning method of CMC was supplied in this paper. Ball-milled CMC nanopowder was successfully electrospun to nanofibers with the assistant of PLA and the presence of NCMC increased the spinnability of PLA. This methodology supplied another option to prepare nanofibers of polymers which are difficult to be electrospun solely. More composite nanofibers could be prepared directly from nanopowders while adopting different raw materials. Owing to the good solubility of NCMC in water, crosslinking is necessary to increase the stability and application possibility of NCMC/PLA mats in biosystem. The crosslinked NCMC/PLA expressed good blood compatibility according to the results of blood clotting time and platelet adhesion experiment. NCMC/PLA is potential to be used in biomaterials, especially as blood-contacting materials.

Acknowledgements This work was supported by the National Science Foundation of China (Project No. 21264007, 21466011). The authors appreciate the financial support.

References

1. Teo AJT, Mishra A, Park I, Kim YJ, Park WT, Yoon YJ (2016) Polymeric biomaterials for medical implants and devices. ACS Biomater Sci Eng 2(4):454–472
2. Kohane DS, Langer R (2010) Biocompatibility and drug delivery systems. Chem Sci 1(4):441–446
3. Weber N, Wendel HP, Ziemer G (2002) Hemocompatibility of heparin-coated surfaces and the role of selective plasma protein adsorption. Biomaterials 2(3):429–439
4. Ercolani E, Gaudio C, Bianco A (2015) Vascular tissue engineering of small-diameter blood vessels: reviewing the electrospinning approach. J Tissue Eng Regen Med 9:861–888
5. Li Q, Dunn E (1992) Applications and properties of chitosan. J Bioact Compat Polym 7:370–397
6. Weber N, Wendel HP, Ziemer G (2002) Hemocompatibility of heparin-coated surfaces and the role of selective plasma protein adsorption. Biomaterials 23:429–439
7. Balan V, Verestiuc L (2014) Strategies to improve chitosan hemocompatibility: a review. Eur Polym 53:171–188
8. Yang Y, Zhou Y, Chuo H, Wang SY, Yu JG (2007) Blood compatibility and mechanical properties of oxidized-chitosan films. J Appl Polym Sci 106:372–377
9. Sharon S, Katanchalee MN (2005) Chitosan based surfactant polymers designed to improve blood compatibility on biomaterials. Colloids Surf B: Biointerfaces 42:147–155

10. Riccardo AAM, Fabio T, Monica E (1984) Sulfated N-(carboxymethyl) chitosans: novel blood anticoagulants. Carbohydr Res 126:225–231
11. Dawei F, Baoqin H, Wen D, Zhao Y, Lv Y, Liu WS (2011) Effects of carboxymethyl chitosan on the blood system of rats. Biochem Biophys Res Commun 408:110–114
12. Zhu AP, Chen T (2006) Blood compatibility of surface-engineered poly(ethylene terephthalate) via o-arboxymethylchitosan. Colloids Surf B: Biointerfaces 50(2):120–125
13. Braghirolli D, Steffens D, Pranke P (2014) Electrospinning for regenerative medicine: a review of the main topics. Drug Discov Today 1(9):743–753
14. Chen H, Song W, Zhou F, Wu ZK, Huang H, Zhang JH, Lin Q, Yang B (2009) The effect of surface microtopography of poly(dimethylsiloxane) on protein adsorption, platelet and cell adhesion. Colloid Surf B 7(1):275–281
15. Doshi J, Reneker DH (1995) Electrospinning and applications of electrospun fibers. J Electrost 3(5):151–160
16. Reneker DH, Chun I (1996) Nanometre diameter fibres of polymer produced by electrospinning. Nanotechnology 7:216–223
17. Ohkawa K, Cha D, Kim H, Nishida A, Yamamoto H (2004) Electrospinning of chitosan. Macromol Rapid Commun 25:1600–1605
18. Theron SA, Yarin AL, Zussman E, Kroll E (2005) Multiple jets in electrospinning: experiment and modeling. Polymer 4(6):2889–2899
19. Ding F, Deng H, Du Y, Shi X, Wang Q (2014) Emerging chitin and chitosan nanofibrous materials for biomedical applications. Nano 6: 9477–9493
20. Kriegel C, Kit K, McClements DJ, Weiss J (2009) Electrospinning of chitosan–poly (ethylene oxide) blend nanofibers in the presence of micellar surfactant solutions. Polymer 50:189–200
21. Du J, Hsieh YL (2008) Nanofibrous membranes from aqueous electrospinning of carboxymethyl chitosan. Nanotechnology19(12): 125707
22. Du F, Wang H, Zhao W, Li D, Kong D, Yang J, Zhang Y (2012) Gradient nanofibrous chitosan/poly −3 caprolactone scaffolds as extracellular microenvironments for vascular tissue engineering. Biomaterials 33:762–770
23. Min BM, Lee SW, Lim JN, You Y, Lee TS, Kang PH, Park WH (2004) Chitin and chitosan nanofibers: electrospinning of chitin and deacetylation of chitin nanofibers. Polymer 45:7137–7142
24. Robert P, Mauduit J, Frank RM, Vert M (1993) Biocompatibility and resorbability of a poly(lactic acid) membrane for periodontal guided tissue regeneration. Biomaterials 14:353–358
25. Tsuji H (2005) Poly(lactide) stereocomplexes: formation, structure, properties, degradation, and applications. Macromol Biosci 5:569–597
26. Michel V (2015) After soft tissues, bone, drug delivery and packaging, PLA aims at blood. Eur Polym J 68:516–552
27. Zhao XW, Lin Y, Phil C, Fin CR, Michasel M (2013) Structure and blood compatibility of highly oriented poly(lactic acid)/thermoplastic polyurethane blends produced by solid hot stretching. Polym Adv Technol 249:853–860
28. Gao AL, Liu F, Xue LX (2014) Preparation and evaluation of heparin-immobilized poly (lactic acid) (PLA) membrane for hemodialysis. J Membr Sci 452:390–399
29. Li ZQ, Zhao XW, Ye L, Coates P, Caton-Rose F (2015) Fibrillation of chain branched poly (lactic acid) with improved blood compatibility and bionic structure. Chem Eng J 279:767–776
30. Chen Y, Lin J, Wan YQ, Fei YN, Wang HB, Gao WD (2012) Preparation and blood compatibility of electrospun PLA/curcumin composite membranes. Polymer 13:1254–1258
31. Reno F, Paul G, Rizzi M, Gatti G, Marchese L (2013) Poly (D,L) lactic acid blending with vitamin e increases polymer hemocompatibility: an hydrophilic effect. J Appl Polym Sci 129(3):1527–1533
32. Zhang W, Zhang JL, Jiang QX, Xia WS (2012) Physicochemical and structural characteristics of chitosan nanopowders prepared by ultrafine milling. Carbohydr Polym 87:309–313
33. Zheng BZ, Liu GY, Yao AW, Xiao YL, Du J, Guo Y, Xiao D, Hu Q, Choi (2014) Sensors & Actuators B Chem 195(5): 431–438
34. Zhang W, Zhang JL, Xia WS (2014) Effect of ball-milling treatment on physicochemical and structural properties of chitosan. Int J Food Prop 17:26–37
35. Hohman MM, Shin M, Rutledge G, Brenner MP (2001) Electrospinning and electrically forced jets: II. Appl Phys Fluids 13:2221
36. Reneker DH, Yarin AL, Fong H, Koombhongse S (2000) Bending instability of electrically charged liquid jets of polymer solutions in elec-trospinning. J Appl Phys 87(4):5–31
37. Theron A, Zussman E, Yarin AL (2004) Experimental investigation of the governing parameters in the electrospinning of polymer solutions. Polymer 45:2017–2030
38. Rouxhet PG, Genet MJ (2011) XPS analysis of bio-organic systems. Surf Interface Anal 43:1453–1470
39. Maachou H, Genet MJ, Aliouche D, Christine C (2013) XPS analysis of chitosan–hydroxyapatite biomaterials: from elements to compounds. Surf Interface Anal 45:1088–1097
40. Yin X, Chen J, Yuan W, Lin Q, Ji L, Liu F (2012) Preparation and antibacterial activity of Schiff bases from O-carboxymethyl chitosan and para-substituted benzaldehydes. Polym Bull 68:1215–1226
41. Hou X, Wang X, Zhu Q, Bao J, Mao C, Jiang L, Shen J (2010) Preparation of polypropylene superhydrophobic surface and its blood compatibility. Colloids Surf B: Biointerfaces 80:247–250
42. Maharana T, Pattanaik S, Routaray A, Nath N, Sutar AK (2015) Synthesis and characterization of poly(lactic acid) based graft copolymers. React Funct Polym 93:47–67
43. Reis EF, Campos FS, Lage AP, Leite RC, Heneine LG, Vasconcelos WL, Lobato ZIP, Mansur HS (2006) Synthesis and characterization of poly (vinyl alcohol) hydrogels and hybrids for rMPB70 protein adsorption. Mater Res 9:185–191
44. Monteiro OA, Airoldi C (1999) Some studies of crosslinking chitosan-glutaraldehyde interaction in a homogeneous system. Int J Biol Macromol 26:119–128
45. Karatum O, Steiner SA, Griffin JS, Shi WB, Plata DL (2016) Mechanically durable aerogel composites for oil capture and recovery. ACS Appl Mater Interfaces 81:215–224
46. Hao PF, Lv C, Yao J, Niu ZH (2014) Wetting property of smooth and textured hydrophobic surfaces under condensation condition. Sci China Phys Mech Astron 57:2127–2132
47. Nie CH, Ma L, Cheng C, Deng J, Zhao CS (2015) Nanofibrous heparin and heparin-mimicking multilayers as highly effective Endothelialization and Antithrombogenic coatings. Biomacromolecules 16:992–1001
48. Nie CX, Ma L, Cheng C, Deng J, Zhao CS (2011) Nanofibrous heparin and heparin-mimicking multilayers as highly effective Endothelialization and Antithrombogenic coatings. Biomacromolecules 16:992–1001
49. Li GC, Yang P, Qin W, Manfred FM, Zhou S, Huang N (2011) The effect of coimmobilizing heparin and fibronectin on titanium on hemocompatibility and endothelialization. Biomaterials 32:4691–4703
50. Esmaeil SLM, Azadeh G, Ahmad FI (2016) Improving blood compatibility of Polyethersulfone hollow fiber membranes via blending with sulfonated polyether ether ketone, Macromol. Mater Eng 1:1–8

51. Jansen AJG, Josefsson CE, Rumjantseva V, Liu QYP, Falet H, Bergmeier W, Cifuni SM, Sackstein R, Von Andrian HU, Wagner DD, Hartwig JH, Hoffmeister KM (2012) Desialylation accelerates platelet clearance after refrigeration and initiates GPIbα metalloproteinase-mediated cleavage in mice. Blood 11(95): 1263–1273

52. Xiang T, Yue WW, Wang R, Liang S, Sun SD, Zhao CS (2013) Surface hydrophilic modification of polyethersulfone membranes by surface-initiated ATRP with enhanced blood compatibility. Colloids Surf B: Biointerfaces 110:15–21